33RD CONGRESS
OF THE INTERNATIONAL COUNCIL
OF THE AERONAUTICAL SCIENCES
STOCKHOLM, SWEDEN, 4-9 SEPTEMBER, 2022

ICAS 2022 SWEDEN

TRANSIENT AND FREE-VIBRATION ANALYSIS OF LAMINATED SHELLS THROUGH THE DISCONTINUOUS GALERKIN METHOD

G. Guarino[1], V. Gulizzi[1,2] & A. Milazzo[1]

[1]University of Palermo, Department of Engineering, V.le delle Scienze, Bld. 8, 90128, Palermo, Italy
[2]Center for Computational Sciences and Engineering, Lawrence Berkeley National Laboratory, 94720, Berkeley, CA, USA

Abstract

This paper presents a novel formulation for linear transient and free-vibration analysis of laminated shell structures based on Interior Penalty discontinuous Galerkin (DG) methods and variable-order through-the-thickness kinematics, whose combined use allows solving the shell problem with high-order accuracy throughout both the shell thickness and the shell modelling domain. The shell geometry is described via a generic system of curvilinear coordinates using either an analytical or a NURBS-based parametrization of the shell mid surface; the formulation also allows for the presence of cut-outs, which are implicitly represented by means of a level set function. After deriving the governing equations of the shell problem from the weak form of three-dimensional elasto-dynamics, the spatial discretization is performed via the DG approach, whereas the temporal time-stepping by the Newmark scheme. Damping of the dynamic system is considered using the classical Rayleigh model. Various numerical tests and the corresponding comparison with reference solutions are provided to assess the accuracy of the proposed formulation.

Keywords: Discontinuous Galerkin methods, transient analysis, free-vibration analysis, composite shells

1. Introduction

In advanced applications for aerospace and automotive industries, laminated shells have become the preferred class of materials thanks to the numerous design/optimization strategies that allows for substantial weight savings and structural performance enhancements. Among the various loading configurations, it is well-known that dynamic loads easily induce larger strain and stress fields than those predicted by static analyses when they excite the natural frequencies of the considered structures [1]. In the context of laminated shells, these fields are significantly affected by the interplay among the inherent heterogeneity, the shell curvature and the possible presence of cut-outs, which render the study of these structures a complex engineering problem that requires the development of accurate numerical models [2, 3, 4, 5]. To maintain a high accuracy while reducing the computational cost, high-order two-dimensional shell formulations are a valid alternative to fully three-dimensional models [6]. An example is provided by Equivalent Single Layer (ESL) theories, see e.g.[7, 6], whereby the components of the displacement field are assumed to vary according to high-order functions throughout the shell thickness. The shell is thus replaced by a single layer that is characterized by equivalent mechanical properties and is governed by a system of differential equations in a set of two curvilinear variables. These governing equations are generally solved via numerical methods as analytical solutions exist only for a limited set of boundary conditions and material properties. Among the numerical approaches proposed in literature, the discontinuous Galerkin (DG) method [8] has proved to be a powerful and flexible technique that offers high-order accuracy for conventional and non-conventional meshes, see e.g.[9, 10, 11], and has been employed successfully for the static analysis of shells [12, 13, 14, 15]. Regarding eigenvalues analysis, DG has been used for problems unrelated to shell structures [16, 17, 18], and more recently for the linear buckling analysis of plates and shells [19]. Nevertheless, to the best of the Authors' knowledge, a DG formulation for the analysis of the linear dynamic regime and of the free-vibrations of multilayered shells is not available in the literature.

In this paper, we present a novel DG formulation for linear transient and free-vibration analysis of laminated shell structures modelled by ESL kinematics. The geometry of the shell is described via a generic system of curvilinear coordinates, while the presence of cut-outs is modelled implicitly by means of a level set function. The DG approach is then employed to discretize the governing equations in space, whereas the temporal time-stepping is performed by a standard Newmark scheme. Damping of the dynamic system is considered using the classical Rayleigh model.
The paper is organized as follows: Sec.2.introduces the two-dimensional weak formulations for the transient and free-vibration analysis of laminated shells structures that are developed starting from the weak forms of the three-dimensional elasto-dynamic and free-vibration problems for a multilayered solid. Subsequently, Sec.3. introduces the domain-partition strategy employed in this work, namely the implicitly-defined mesh technique [20, 21], and the proposed Interior Penalty DG method for transient and free-vibration analysis of shells. In Sec.4.the accuracy of the proposed formulation is assessed by computing the transient response and the natural frequencies of plates and cylindrical shells, for which analytical and semi-analytical solutions are available. Then, the formulation is employed to study a multilayered shell whose geometry is represented via a NURBS parametrization and the obtained results are compared with those computed using Abaqus. The comparison confirms the accuracy and the flexibility of the proposed approach.

2. Formulation

Let us consider a shell consisting of N_ℓ linear-elastic, homogeneous, orthotropic layers. A quantity relative to the ℓ-th layer is denoted by the superscript $\langle\ell\rangle$ that takes values in $1,\dots,N_\ell$. Each layer is characterized by its thickness $\tau^{\langle\ell\rangle}$ and its lamination angle $\theta^{\langle\ell\rangle}$, which are assumed to be uniform. The volume of the shell $V \subset \mathbb{R}^3$ is obtained as the union of the volumes of the layers and its boundary is denoted as ∂V. Thus, the thickness of the shell is $\tau = \sum_{\ell=1}^{N_\ell} \tau^{\langle\ell\rangle}$. Eventually, in the reminder of the paper, Einstein summation convection is employed, where Latin indices span the set $\{1,2,3\}$ and Greek indices span the set $\{1,2\}$.

2.1 Geometry description

The geometrical description of the shell starts from the map of its mid surface S that is represented by the following equation

$$\boldsymbol{x}_0 = \boldsymbol{x}_0(\xi_1,\xi_2), \quad \text{for } (\xi_1,\xi_2) \in \Omega_\xi. \tag{1}$$

where $\boldsymbol{x}_0 = (x_{01},x_{02},x_{03})^\intercal$ is a generic point of S, ξ_1 and ξ_2 are auxiliary curvilinear coordinates and $\Omega_\xi \subset \mathbb{R}^2$ is the so-called *reference domain*. A normal unit vector $\boldsymbol{n}_0$ is associated to each point of S and is computed as

$$\boldsymbol{n}_0 \equiv \frac{\boldsymbol{a}_1 \times \boldsymbol{a}_2}{||\boldsymbol{a}_1 \times \boldsymbol{a}_2||}, \tag{2}$$

where

$$\boldsymbol{a}_1 \equiv \frac{\partial \boldsymbol{x}_0}{\partial \xi_1} \quad \text{and} \quad \boldsymbol{a}_2 \equiv \frac{\partial \boldsymbol{x}_0}{\partial \xi_2}. \tag{3}$$

Upon introducing a third curvilinear variable $\xi_3 \in I_{\xi_3}$, where $I_{\xi_3} \equiv [-\tau/2, \tau/2]$, the generic point $\boldsymbol{x}$ of the shell volume V is given by the map

$$\boldsymbol{x} = \boldsymbol{x}(\xi_1,\xi_2,\xi_3) \equiv \boldsymbol{x}_0(\xi_1,\xi_2) + \xi_3 \boldsymbol{n}_0(\xi_1,\xi_2), \quad \text{for } (\xi_1,\xi_2,\xi_3) \in \Omega_\xi \times I_{\xi_3}. \tag{4}$$

Using Eq.(4), the vectors $\boldsymbol{g}_i$ of the local covariant basis are obtained as $\boldsymbol{g}_i \equiv \partial \boldsymbol{x}/\partial \xi_i$, while the vectors $\boldsymbol{g}^i$ of the local contravariant basis are defined implicitly as $\boldsymbol{g}^i \cdot \boldsymbol{g}_j = \delta^i_j$, where δ^i_j is the Kronecker delta. Additionally, the covariant components of the metric tensor are defined as $g_{ij} \equiv \boldsymbol{g}_i \cdot \boldsymbol{g}_j$, its contravariant components as $g^{ij} \equiv \boldsymbol{g}^i \cdot \boldsymbol{g}^j$ and the determinant of (g_{ij}) is denoted as g. Collecting the vector of the contravariant basis as columns of the matrix $\boldsymbol{R}_\xi$, the following relationship holds

$$\boldsymbol{v} = \boldsymbol{R}_\xi \boldsymbol{v}_\xi, \tag{5}$$

where $\boldsymbol{v} \equiv (v_1,v_2,v_3)^\intercal$ collects the Cartesian components of a generic vector in $\mathbb{R}^3$, whereas $\boldsymbol{v}_\xi \equiv (v_{\xi_1},v_{\xi_2},v_{\xi_3})^\intercal$ contains the corresponding covariant components. For further details on the differential geometry employed in this work, the reader is referred to [22].

Finally, the volume of the ℓ-th layer, denoted as $V^{\langle\ell\rangle}$, is identified as the region of the volume of the shell where ξ_3 varies between a bottom value $\xi_{3b}^{\langle\ell\rangle}$ and a top value $\xi_{3t}^{\langle\ell\rangle}$. As such, it results $\xi_{3t}^{\langle\ell\rangle} - \xi_{3b}^{\langle\ell\rangle} = \tau^{\langle\ell\rangle}$ and $\xi_{3t}^{\langle\ell-1\rangle} = \xi_{3b}^{\langle\ell\rangle}$ for $\ell = 2,\dots,N_\ell$.

2.2 NURBS-based surface

As introduced in Sec.2.1, the mid surface of the shell is defined starting from a map $\boldsymbol{x}_0 = \boldsymbol{x}_0(\xi_1,\xi_2)$. In this work, either analytical functions or NURBS functions are used for this scope. The use of the latter facilitates the coupling of the present formulation with CAD software libraries and allows reproducing complex shapes with high-order continuity. The starting point to construct a NURBS sururface is a grid of $(n+1)\times(m+1)$ so-called *control points*. The map of the mid surface is therefore defined as

$$\boldsymbol{x}_0(\xi_1,\xi_2) \equiv \sum_{i=1}^{n+1}\sum_{j=1}^{m+1} \boldsymbol{P}_{ij} S_{ij}(\xi_1,\xi_2), \tag{6}$$

where $\boldsymbol{P}_{ij}$ is a generic control point and $S_{ij}(\xi_1,\xi_2)$ is the associated *shape function*. The generic shape functions is defined as

$$S_{ij}(\xi_1,\xi_2) = \frac{h_{ij} N_{i,k}(\xi_1) M_{j,l}(\xi_2)}{\sum_{i=1}^{n+1}\sum_{j=1}^{m+1} h_{ij} N_{i,k}(\xi_1) M_{j,l}(\xi_2)}, \tag{7}$$

where h_{ij} is the weight associated to the control point $\boldsymbol{P}_{ij}$, $N_{i,k}(\xi_1)$ is the one dimensional i-th B-spline function in the direction ξ_1 having order k and $M_{j,l}(\xi_2)$ is the one-dimensional j-th B-spline basis function in the direction ξ_2 having order l. The Cox de Boor formula is used to define the B-spline functions as

$$N_{i,1}(\xi) = \begin{cases} 1 & \text{for } \xi^i \le \xi \le \xi^{i+1} \\ 0 & \text{otherwise} \end{cases}, \tag{8a}$$

$$N_{i,k}(\xi) = \frac{(\xi - \xi^i) N_{i,k-1}(\xi)}{\xi^{i+k-1} - \xi^i} + \frac{(\xi^{i+k} - \xi) N_{i+1,k-1}(\xi)}{\xi^{i+k} - \xi^{i+1}}, \tag{8b}$$

where the values of ξ^i are taken from the so-called *knot vector* $\left\{\xi^1,\xi^2,\dots,\xi^i,\dots,\xi^{n+k+1}\right\}$ that identifies the intervals for the piece-wise definition of the B-spline. For further details on NURBS surfaces the interested reader is referred to the books by Rogers [28] and by Piegl and Tiller [29].

2.3 The Equivalent-Single-Layer theory

Within the Equivalen-Single-Layer (ESL) theories, the whole laminate is treated in an unique fashion by expanding the mechanical variables of interest via the same functions throughout all the layers. In this work, a displacement based formulation is adopted and the expansion is performed for the covariant components of the displacement vector $\boldsymbol{u}_\xi \equiv (u_{\xi_1}, u_{\xi_2}, u_{\xi_3})^\mathsf{T}$, such that one may write

$$u_{\xi_i}(\xi_1,\xi_2,\xi_3) = \sum_{k=0}^{N_i} Z_k^i(\xi_3) U_k^i(\xi_1,\xi_2), \tag{9}$$

where $Z_k^i(\xi_3)$ is the k-th known function of the third curvilinear coordinate, $U_k^i(\xi_1,\xi_2)$ is the k-th so-called *generalized displacement*, N_i is the order of expansion of u_{ξ_i}. The generalized displacements are collected in a vector $\boldsymbol{U}$, whose dimension is $N_U = N_1 + N_2 + N_3 + 3$. Similarly the functions $Z_k^i(\xi_3)$ are consistently collected in a $3\times N_U$ matrix $\boldsymbol{Z}$ such that the vector of covariant displacement components may be written in matrix form as follows

$$\boldsymbol{u}_\xi = \boldsymbol{Z}(\xi_3)\boldsymbol{U}(\xi_1,\xi_2). \tag{10}$$

2.4 Strain-displacements relationship

Let γ be the strain tensor in Voigt notation, i.e. $\gamma = (\gamma_{11}, \gamma_{22}, \gamma_{33}, \gamma_{23}, \gamma_{13}, \gamma_{12})^\intercal$. Introducing the Cartesian components of the displacement vector $\boldsymbol{u} = (u_1, u_2, u_3)^\intercal$, the relationship between the strain and the displacement is expressed, within the small displacements hypothesis, as

$$\boldsymbol{\gamma} = \boldsymbol{I}_i \frac{\partial \boldsymbol{u}}{\partial x_i}, \tag{11}$$

where the following auxiliary matrices have been introduced

$$\boldsymbol{I}_1 \equiv \begin{bmatrix} 1 & 0 & 0 \\ 0 & 0 & 0 \\ 0 & 0 & 0 \\ 0 & 0 & 0 \\ 0 & 0 & 1 \\ 0 & 1 & 0 \end{bmatrix}, \quad \boldsymbol{I}_2 \equiv \begin{bmatrix} 0 & 0 & 0 \\ 0 & 1 & 0 \\ 0 & 0 & 0 \\ 0 & 0 & 1 \\ 0 & 0 & 0 \\ 1 & 0 & 0 \end{bmatrix} \quad \text{and} \quad \boldsymbol{I}_3 \equiv \begin{bmatrix} 0 & 0 & 0 \\ 0 & 0 & 0 \\ 0 & 0 & 1 \\ 0 & 1 & 0 \\ 1 & 0 & 0 \\ 0 & 0 & 0 \end{bmatrix}. \tag{12}$$

Then, the Cartesian coordinates of the displacement vector are related to the covariant ones by means of Eq.(5). Using Eq.(10), it is possible to show that the derivatives of the displacement in Cartesian components are related to the generalized displacement vector $\boldsymbol{U}$ and its derivatives with respect to ξ_α as

$$\frac{\partial \boldsymbol{u}}{\partial x_i} = \boldsymbol{D}_{0i}\boldsymbol{U} + \boldsymbol{D}_{\alpha i}\frac{\partial \boldsymbol{U}}{\partial \xi_\alpha}, \tag{13}$$

where

$$\boldsymbol{D}_{0i} \equiv \frac{\partial \xi_j}{\partial x_i}\frac{\partial \boldsymbol{R}_\xi}{\partial \xi_j}\boldsymbol{Z} + \frac{\partial \xi_3}{\partial x_i}\boldsymbol{R}_\xi \frac{\mathrm{d}\boldsymbol{Z}}{\mathrm{d}\xi_3}, \quad \text{and} \quad \boldsymbol{D}_{\alpha i} \equiv \frac{\partial \xi_\alpha}{\partial x_i}\boldsymbol{R}_\xi \boldsymbol{Z}. \tag{14}$$

Finally, upon using Eq.(13) in Eq.(11), the strain vector γ is written as

$$\boldsymbol{\gamma} = \boldsymbol{J}_0\boldsymbol{U} + \boldsymbol{J}_\alpha \frac{\partial \boldsymbol{U}}{\partial \xi_\alpha}, \tag{15}$$

where

$$\boldsymbol{J}_0 \equiv \boldsymbol{I}_i\boldsymbol{D}_{0i} \quad \text{and} \quad \boldsymbol{J}_\alpha \equiv \boldsymbol{I}_i\boldsymbol{D}_{\alpha i}. \tag{16}$$

2.5 Constitutive behaviour

The constitutive behavior of the considered composite laminated shells is determined starting from the constitutive behavior of the layers, which are assumed to be orthotropic, linear-elastic, and homogeneous. As such, in the basis $\boldsymbol{m}_1^{\langle \ell \rangle}$, $\boldsymbol{m}_2^{\langle \ell \rangle}$ and $\boldsymbol{m}_3^{\langle \ell \rangle}$ aligned with the ℓ-th layer's fibers direction, the layer's behavior may be characterized using the engineering constants, i.e. Young's moduli, Poisson ratios and shear moduli [31]. The basis of orthotropic material behavior is defined as

$$\boldsymbol{m}_1^{\langle \ell \rangle} \equiv \boldsymbol{R}_{\boldsymbol{n}_0}(\theta^{\langle \ell \rangle})\frac{\boldsymbol{g}_1}{||\boldsymbol{g}_1||}, \quad \boldsymbol{m}_3^{\langle \ell \rangle} \equiv \boldsymbol{n}_0, \quad \text{and} \quad \boldsymbol{m}_2^{\langle \ell \rangle} \equiv \boldsymbol{m}_3^{\langle \ell \rangle} \times \boldsymbol{m}_1^{\langle \ell \rangle}, \tag{17}$$

where $\boldsymbol{R}_{\boldsymbol{n}_0}(\theta^{\langle \ell \rangle})$ is the matrix that performs a rotation of the lamination angle $\theta^{\langle \ell \rangle}$ around the axis identified by $\boldsymbol{n}_0$. In this reference system the constitutive relationship is expressed as

$$\widetilde{\boldsymbol{\sigma}}^{\langle \ell \rangle} = \widetilde{\boldsymbol{c}}^{\langle \ell \rangle}\widetilde{\boldsymbol{\gamma}}^{\langle \ell \rangle}, \tag{18}$$

where $\widetilde{\boldsymbol{\sigma}}^{\langle \ell \rangle}$, is the stress tensor in Voigt notation, $\widetilde{\boldsymbol{\gamma}}^{\langle \ell \rangle}$ is the strain tensor in Voigt notation and $\widetilde{\boldsymbol{c}}^{\langle \ell \rangle}$ is the constitutive matrix. The constitutive relationship is expressed in Cartesian coordinates by expressing the constitutive matrix in a rotated coordinate system via standard transformation rules, see e.g. [30]. In such way, one may write

$$\boldsymbol{\sigma}^{\langle \ell \rangle} = \boldsymbol{c}^{\langle \ell \rangle}\boldsymbol{\gamma}, \tag{19}$$

where $\boldsymbol{\sigma}^{\langle \ell \rangle}$, $\boldsymbol{\gamma}$, and $\boldsymbol{c}^{\langle \ell \rangle}$ are the stress, the strain and the constitutive matrix in Cartesian coordinates respectively. Note that the strain $\boldsymbol{\gamma}$ is given by Eq.(15) and is the same for all the layers of the shell, whereas $\boldsymbol{\sigma}^{\langle \ell \rangle}$ is typically discontinuous across the layers.

2.6 Transient analysis

The governing equations of transient analysis of a multilayered shell are derived starting from the weak form of the elasto-dynamic problem of a three-dimensional structure consisting of N_ℓ layers, which reads

$$\sum_{\ell=1}^{N_\ell}\int_{V^{\langle\ell\rangle}}\delta\boldsymbol{u}^\intercal\rho^{\langle\ell\rangle}\ddot{\boldsymbol{u}}\mathrm{d}V+\sum_{\ell=1}^{N_\ell}\int_{V^{\langle\ell\rangle}}\delta\boldsymbol{\gamma}^\intercal\boldsymbol{\sigma}^{\langle\ell\rangle}\mathrm{d}V=\sum_{\ell=1}^{N_\ell}\int_{V^{\langle\ell\rangle}}\delta\boldsymbol{u}^\intercal\overline{\boldsymbol{b}}\mathrm{d}V+\sum_{\ell=1}^{N_\ell}\int_{\partial V^{\langle\ell\rangle}}\delta\boldsymbol{u}^\intercal\overline{\boldsymbol{t}}\mathrm{d}\partial V. \tag{20}$$

In Eq.(20), $\rho^{\langle\ell\rangle}$ is the density of the ℓ-th layer, $\boldsymbol{\gamma}$ and $\boldsymbol{\sigma}^{\langle\ell\rangle}$ are the strain and the stress fields in Voigt notation, respectively, $\ddot{\boldsymbol{u}}$ is the second derivative of $\boldsymbol{u}$ with respect to time, $\overline{\boldsymbol{t}}$ is the vector of prescribed traction on the external surface and $\overline{\boldsymbol{b}}$ is the vector of prescribed external volume forces. It is worth noting that, although no damping terms are present in Eq.(20), they will be introduced within the formulation via the Rayleigh damping method as detailed in Sec. 3. Using Eqs.(19) and (15), it is possible to obtain the following weak formulation for the transient analysis of laminated shells in terms of the vector $\boldsymbol{U}$ of generalized displacements

$$\int_{\Omega_\xi}\delta\boldsymbol{U}^\intercal\boldsymbol{M}\ddot{\boldsymbol{U}}\mathrm{d}\Omega_\xi+\int_{\Omega_\xi}\left[\frac{\partial\delta\boldsymbol{U}^\intercal}{\partial\xi_\alpha}\left(\boldsymbol{Q}_{\alpha\beta}\frac{\partial\boldsymbol{U}}{\partial\xi_\beta}+\boldsymbol{R}_{\alpha3}\boldsymbol{U}\right)+\delta\boldsymbol{U}^\intercal\left(\boldsymbol{R}_{\alpha3}^\intercal\frac{\partial\boldsymbol{U}}{\partial\xi_\alpha}+\boldsymbol{S}_{33}\boldsymbol{U}\right)\right]\mathrm{d}\Omega_\xi=\int_{\Omega_\xi}\delta\boldsymbol{U}^\intercal\overline{\boldsymbol{B}}\,\mathrm{d}\Omega_\xi+\int_{\partial\Omega_\xi}\delta\boldsymbol{U}^\intercal\overline{\boldsymbol{T}}\,\mathrm{d}\partial\Omega_\xi, \tag{21}$$

where the matrices $\boldsymbol{Q}_{\alpha\beta}$, $\boldsymbol{R}_{\alpha3}$, and $\boldsymbol{S}_{33}$ are referred to as *generalized stiffness matrices* and are defined as

$$\boldsymbol{Q}_{\alpha\beta}\equiv\sum_{\ell=1}^{N_\ell}\int_{\xi_{3b}^{\langle\ell\rangle}}^{\xi_{3t}^{\langle\ell\rangle}}\boldsymbol{J}_\alpha^\intercal\boldsymbol{c}^{\langle\ell\rangle}\boldsymbol{J}_\beta\sqrt{g}\,\mathrm{d}\xi_3, \tag{22a}$$

$$\boldsymbol{R}_{\alpha3}\equiv\sum_{\ell=1}^{N_\ell}\int_{\xi_{3b}^{\langle\ell\rangle}}^{\xi_{3t}^{\langle\ell\rangle}}\boldsymbol{J}_\alpha^\intercal\boldsymbol{c}^{\langle\ell\rangle}\boldsymbol{J}_0\sqrt{g}\,\mathrm{d}\xi_3, \tag{22b}$$

$$\boldsymbol{S}_{33}\equiv\sum_{\ell=1}^{N_\ell}\int_{\xi_{3b}^{\langle\ell\rangle}}^{\xi_{3t}^{\langle\ell\rangle}}\boldsymbol{J}_0^\intercal\boldsymbol{c}^{\langle\ell\rangle}\boldsymbol{J}_0\sqrt{g}\,\mathrm{d}\xi_3. \tag{22c}$$

The matrix $\boldsymbol{M}$ is referred to as *generalized mass matrix* and is defined as

$$\boldsymbol{M}\equiv\sum_{\ell=1}^{N_\ell}\int_{\xi_{3b}^{\langle\ell\rangle}}^{\xi_{3t}^{\langle\ell\rangle}}\boldsymbol{Z}^\intercal\boldsymbol{R}_\xi^\intercal\boldsymbol{R}_\xi\boldsymbol{Z}\rho^{\langle\ell\rangle}\sqrt{g}\,\mathrm{d}\xi_3. \tag{23}$$

Finally, $\overline{\boldsymbol{B}}$ and $\overline{\boldsymbol{T}}$ are the *generalized volume loads* and the *generalized boundary loads* and are given as

$$\overline{\boldsymbol{B}}\equiv\left(\boldsymbol{Z}^\intercal\boldsymbol{R}_\xi^\intercal\overline{\boldsymbol{t}}\sqrt{g}\sqrt{n_ig^{ij}n_j}\right)_{\xi_3=\pm\tau/2}+\int_{-\tau/2}^{\tau/2}\boldsymbol{Z}^\intercal\boldsymbol{R}_\xi^\intercal\overline{\boldsymbol{b}}\sqrt{g}\,\mathrm{d}\xi_3, \tag{24a}$$

$$\overline{\boldsymbol{T}}\equiv\int_{-\tau/2}^{\tau/2}\boldsymbol{Z}^\intercal\boldsymbol{R}_\xi^\intercal\overline{\boldsymbol{t}}\sqrt{g}\sqrt{n_ig^{ij}n_j}\,\mathrm{d}\xi_3. \tag{24b}$$

2.7 Free-vibration analysis

Similarly to the case discussed in the preceding section, the equations governing the free-vibration analysis of a laminated shell are derived from the following weak form of a three-dimensional multi-layered structure

$$\sum_{\ell=1}^{N_\ell}\int_{V^{\langle\ell\rangle}}\delta\boldsymbol{\gamma}^\intercal\boldsymbol{\sigma}^{\langle\ell\rangle}\mathrm{d}V=\omega^2\sum_{\ell=1}^{N_\ell}\int_{V^{\langle\ell\rangle}}\delta\boldsymbol{u}^\intercal\rho^{\langle\ell\rangle}\boldsymbol{u}\mathrm{d}V, \tag{25}$$

where ω is a generic natural frequency. Upon applying the same substitutions as in Sec.2.6 the corresponding two-dimensional shell formulation is obtained

$$\int_{\Omega_\xi}\left[\frac{\partial\delta\boldsymbol{U}^\intercal}{\partial\xi_\alpha}\left(\boldsymbol{Q}_{\alpha\beta}\frac{\partial\boldsymbol{U}}{\partial\xi_\beta}+\boldsymbol{R}_{\alpha3}\boldsymbol{U}\right)+\delta\boldsymbol{U}^\intercal\left(\boldsymbol{R}_{\alpha3}^\intercal\frac{\partial\boldsymbol{U}}{\partial\xi_\alpha}+\boldsymbol{S}_{33}\boldsymbol{U}\right)\right]\mathrm{d}\Omega_\xi=\omega^2\int_{\Omega_\xi}\delta\boldsymbol{U}^\intercal\boldsymbol{M}\boldsymbol{U}\mathrm{d}\Omega_\xi \tag{26}$$

3. Discontinuous Galerkin formulation

In a DG formulation, the reference domain Ω_ξ is partitioned into N_e elements such that $\Omega_\xi^h \equiv \bigcup_{e=1}^{N_e} \Omega_\xi^e \approx \Omega_\xi$, where Ω_ξ^e is a generic mesh element. The collections of the boundaries of the elements where Dirichlet and Neumann boundary conditions are enforced are denoted as $\partial\Omega_{\xi D}^h$ and $\partial\Omega_{\xi N}^h$, respectively. Additionally, the partitioning of the domain creates N_i inter-element interfaces that are collected in $\partial\Omega_{\xi I}^h \equiv \bigcup_{i=1}^{N_i} \partial\Omega_\xi^i$, being $\partial\Omega_\xi^i$ a generic i-th interface. The so-called *broken integrals* are thus introduced

$$\int_{\Omega_\xi^h} \bullet \equiv \sum_{e=1}^{N_e} \int_{\Omega_\xi^e} \bullet^e \, \mathrm{d}\Omega_\xi, \tag{27a}$$

$$\int_{\partial\Omega_{\xi I}^h} \bullet \equiv \sum_{i=1}^{N_i} \int_{\partial\Omega_{\xi I}^i} \bullet^i \, \mathrm{d}\partial\Omega_\xi, \tag{27b}$$

$$\int_{\partial\Omega_{\xi D}^h} \bullet \equiv \sum_{e=1}^{N_e} \int_{\partial\Omega_{\xi D}^e} \bullet^e \, \mathrm{d}\partial\Omega_\xi, \tag{27c}$$

$$\int_{\partial\Omega_{\xi N}^h} \bullet \equiv \sum_{e=1}^{N_e} \int_{\partial\Omega_{\xi N}^e} \bullet^e \, \mathrm{d}\partial\Omega_\xi. \tag{27d}$$

Moreover, upon considering two neighboring vectors e and e' and indicating the element's outer unit normal as $\boldsymbol{\nu}^e = (\nu_1^e, \nu_2^e)$, the following *average* and *jump* operators are introduced

$$\{\bullet\}^i \equiv \frac{1}{2}\left(\bullet^e + \bullet^{e'}\right) \quad \text{and} \quad [\![\bullet]\!]_\alpha^i \equiv \nu_\alpha^e \bullet^e + \nu_\alpha^{e'} \bullet^{e'}. \tag{28}$$

3.1 Implicitly-defined mesh

The reference domain is defined as the intersection of a background rectangle $\Pi_\xi \supseteq \Omega_\xi$ having boundary $\partial\Pi_\xi$ and a level set function $\varphi = \varphi(\boldsymbol{x}_0(\xi_1, \xi_2))$. In particular, the reference domain and its boundary are defined as

$$\Omega_\xi \equiv \left\{(\xi_1, \xi_2) \in \Pi_\xi \mid \varphi(\xi_1, \xi_2) < 0\right\} \tag{29a}$$

$$\partial\Omega_\xi \equiv \left\{(\xi_1, \xi_2) \in \partial\Pi_\xi \mid \varphi(\xi_1, \xi_2) < 0\right\} \cup \left\{(\xi_1, \xi_2) \in \Pi_\xi \mid \varphi(\xi_1, \xi_2) = 0\right\}, \tag{29b}$$

The reference rectangle is then partitioned by a structured rectangular-based grid. The intersection between the background grid and the reference domain produces cells that are classified as entire, partial or empty according to weather they lay entirely or partially in the reference domain or do not belong to it. Amongst the partial cells, some may have an unacceptably small area that causes an ill-conditioning of the final linear systems. These cells are merged with nearby entire or partial cells leading to the extended elements. An example of an implicitly-defined mesh, which includes entire, partial and extended elements, is shown in Fig.(1)

3.2 Discontinuous Galerkin for transient analysis

The DG problem related to transient dynamic analysis consists in finding $\boldsymbol{U}_h$ such as

$$B^D(\boldsymbol{V}, \boldsymbol{U}_h, \ddot{\boldsymbol{U}}_h) = F(\boldsymbol{V}, \overline{\boldsymbol{B}}, \overline{\boldsymbol{T}}, \overline{\boldsymbol{U}}), \quad \forall \boldsymbol{V} \in \mathscr{V}_{hp}^{N_U}, \tag{30}$$

where $\mathscr{V}_{hp}$ denotes the space of discontinuous basis functions defined as

$$\mathscr{V}_{hp} \equiv \left\{v : \Omega_\xi^h \to \mathbb{R} \mid v|_{\Omega_\xi^e} \in \mathscr{P}_p^e \; \forall e = 1, ..., N_e\right\}, \tag{31}$$

being $\mathscr{P}_p^e$ the space of poynomials of degree p defined in Ω_ξ^e. Consistently, the space of discontinuous vector basis functions is defined as $\mathscr{V}_{hp}^N \equiv (\mathscr{V}_{hp})^N$. The bilinear form $B^D(\boldsymbol{V}, \boldsymbol{U}_h, \ddot{\boldsymbol{U}}_h)$ and the linear form

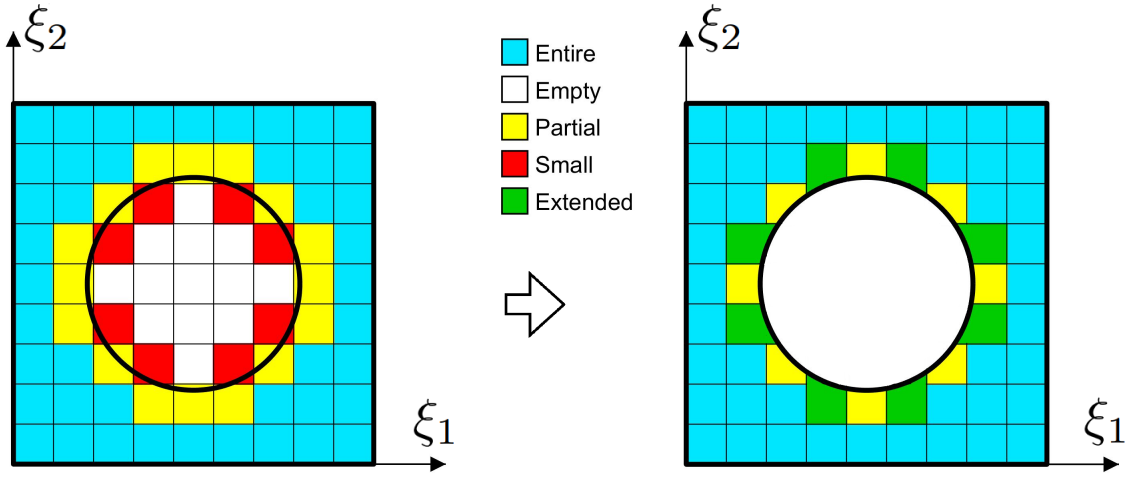

(a) (b)

Figure 1 – (a) Different types of cells. (b) Types of elements of the Implicitly-defined mesh.

$F(\boldsymbol{V},\overline{\boldsymbol{B}},\overline{\boldsymbol{T}},\overline{\boldsymbol{U}})$ in Eq.(30) are defined as

$$\begin{aligned} B^D(\boldsymbol{V},\boldsymbol{U}_h,\ddot{\boldsymbol{U}}_h) \equiv & \int_{\Omega^h_\xi} \boldsymbol{V}^\intercal \boldsymbol{M}\ddot{\boldsymbol{U}}_h + \int_{\Omega^h_\xi} \frac{\partial \boldsymbol{V}^\intercal}{\partial \xi_\alpha}\left(\boldsymbol{Q}_{\alpha\beta}\frac{\partial \boldsymbol{U}_h}{\partial \xi_\beta} + \boldsymbol{R}_{\alpha 3}\boldsymbol{U}_h\right) + \boldsymbol{V}^\intercal\left(\boldsymbol{R}^\intercal_{\alpha 3}\frac{\partial \boldsymbol{U}_h}{\partial \xi_\alpha} + \boldsymbol{S}_{33}\boldsymbol{U}_h\right) + \\ & - \int_{\partial\Omega^h_{\xi I}} [\![\boldsymbol{V}]\!]^\intercal_\alpha \left\{\boldsymbol{Q}_{\alpha\beta}\frac{\partial \boldsymbol{U}_h}{\partial \xi_\beta} + \boldsymbol{R}_{\alpha 3}\boldsymbol{U}_h\right\} + \left\{\frac{\partial \boldsymbol{V}^\intercal}{\partial \xi_\alpha}\boldsymbol{Q}_{\alpha\beta} + \boldsymbol{V}^\intercal\boldsymbol{R}^\intercal_{\beta 3}\right\}[\![\boldsymbol{U}_h]\!]_\beta + \\ & - \int_{\partial\Omega^h_{\xi D}} \nu_\alpha \boldsymbol{V}^\intercal\left(\boldsymbol{Q}_{\alpha\beta}\frac{\partial \boldsymbol{U}_h}{\partial \xi_\beta} + \boldsymbol{R}_{\alpha 3}\boldsymbol{U}_h\right) + \left(\frac{\partial \boldsymbol{V}^\intercal}{\partial \xi_\alpha}\boldsymbol{Q}_{\alpha\beta} + \boldsymbol{V}^\intercal\boldsymbol{R}^\intercal_{\beta 3}\right)\boldsymbol{U}_h\nu_\beta + \\ & + \int_{\partial\Omega^h_{\xi I}} \mu [\![\boldsymbol{V}]\!]^\intercal_\alpha [\![\boldsymbol{U}_h]\!]_\alpha + \int_{\partial\Omega^h_{\xi D}} \mu \boldsymbol{V}^\intercal \boldsymbol{U}_h, \end{aligned} \tag{32}$$

and

$$F(\boldsymbol{V},\overline{\boldsymbol{B}},\overline{\boldsymbol{T}},\overline{\boldsymbol{U}}) \equiv \int_{\Omega^h_\xi} \boldsymbol{V}^\intercal\overline{\boldsymbol{B}} + \int_{\partial\Omega^h_{\xi N}} \boldsymbol{V}^\intercal\overline{\boldsymbol{T}} - \int_{\partial\Omega^h_{\xi D}}\left(\frac{\partial \boldsymbol{V}^\intercal}{\partial \xi_\alpha}\boldsymbol{Q}_{\alpha\beta} + \boldsymbol{V}^\intercal\boldsymbol{R}^\intercal_{\beta 3}\right)\overline{\boldsymbol{U}}\nu_\beta + \int_{\partial\Omega^h_{\xi D}} \mu \boldsymbol{V}^\intercal\overline{\boldsymbol{U}}, \tag{33}$$

respectively. It is worth noting that, in Eqs.(32) and (33), the integrals on $\partial\Omega^h_{\xi D}$ are used to enforce the Dirichlet boundary conditions in terms of prescribed displacements $\overline{\boldsymbol{U}}$, the integrals on $\partial\Omega^h_{\xi N}$ are used to enforce the Neumann boundary conditions and the integrals on $\partial\Omega^h_{\xi I}$ are used to enforce the inter-element continuity; eventually, μ is the so-called *penalty parameter* that must be positive and chosen proportional to Q/h where Q is a sufficiently large constant and h is the characteristic mesh size [8].
Once the DG-based space discretization is introduced in Eq.(30), one obtains the following linear system of second-order differential equations involving only time derivatives

$$\mathscr{M}\ddot{\boldsymbol{X}} + \mathscr{D}\dot{\boldsymbol{X}} + \mathscr{K}\boldsymbol{X} = \boldsymbol{F}, \tag{34}$$

where $\mathscr{M}$, $\mathscr{D}$ and $\mathscr{K}$ are the *mass matrix*, the *damping matrix* and the *stiffness matrix* of the system, respectively, $\boldsymbol{X}$ is the vector containing the problem unknowns and $\dot{\boldsymbol{X}}$ and $\ddot{\boldsymbol{X}}$ are its first and second time derivatives, respectively. It is worth noting that the second term in Eq.(34) does not come directly from Eq.(33); instead, it is introduced to model the damping in the structure. In particular, using Rayleigh damping method, see e.g.[23], the matrix $\mathscr{D}$ is constructed as a linear combination of the matrices $\mathscr{M}$ and $\mathscr{K}$ as

$$\mathscr{D} \equiv \alpha\mathscr{M} + \beta\mathscr{K}. \tag{35}$$

Table 1 – Properties of the considered materials.

Material ID	Property	Component	Value
M_1	Young's moduli	E/E_r	1
	Poisson's ratios	ν	0.25
	Density	ρ/ρ_r	1
M_2	Young's moduli	E_1/E_r	25
		E_2/E_r, E_3/E_r	1
	Poisson's ratios	ν_{23}, ν_{13}, ν_{12}	0.25
	Shear moduli	G_{23}/E_r	0.2
		G_{13}/E_r, G_{12}/E_r	0.5
	Density	ρ/ρ_r	1

where the coefficients α and β are obtained by specifying the damping ratios ζ_i and ζ_j for the i-th and j-th mode and solving the system

$$\frac{1}{2}\begin{bmatrix} \frac{1}{\omega_i} & \omega_i \\ \frac{1}{\omega_j} & \omega_j \end{bmatrix} \begin{bmatrix} \alpha \\ \beta \end{bmatrix} \equiv \begin{bmatrix} \zeta_i \\ \zeta_j \end{bmatrix}. \tag{36}$$

Finally, the temporal time-stepping is solved employing the Newmark integration scheme which, for the sake of conciseness, it is not reported here but may be found in [32].

3.3 Discontinuous Galerkin for free-vibration analysis

For free-vibration analysis, the DG problem becomes finding the eigenvalues $\lambda_h = \frac{1}{\omega_h^2}$ and the eigenfunctions $\boldsymbol{U}_h$ that are solution of the following eigenproblem

$$B^{\Omega}(\boldsymbol{V},\boldsymbol{U}_h) = \frac{1}{\omega_h^2} B(\boldsymbol{V},\boldsymbol{U}_h), \quad \forall \boldsymbol{V} \in \mathscr{V}_{hp}^{N_U}, \tag{37}$$

where ω_h is an approximation of the free-vibration frequencies ω and the following two bilinear forms have been introduced

$$B^{\Omega}(\boldsymbol{V},\boldsymbol{U}_h) \equiv \int_{\Omega_\xi^h} \boldsymbol{V}^\intercal \boldsymbol{M} \boldsymbol{U}_h, \tag{38}$$

and

$$\begin{aligned} B(\boldsymbol{V},\boldsymbol{U}_h) \equiv \int_{\Omega_\xi^h} \frac{\partial \boldsymbol{V}^\intercal}{\partial \xi_\alpha}\left(\boldsymbol{Q}_{\alpha\beta}\frac{\partial \boldsymbol{U}_h}{\partial \xi_\beta} + \boldsymbol{R}_{\alpha 3}\boldsymbol{U}_h\right) + \boldsymbol{V}^\intercal\left(\boldsymbol{R}_{\alpha 3}^\intercal \frac{\partial \boldsymbol{U}_h}{\partial \xi_\alpha} + \boldsymbol{S}_{33}\boldsymbol{U}_h\right) + \\ - \int_{\partial\Omega_{\xi I}^h} [\![\boldsymbol{V}]\!]_\alpha^\intercal \left\{\boldsymbol{Q}_{\alpha\beta}\frac{\partial \boldsymbol{U}_h}{\partial \xi_\beta} + \boldsymbol{R}_{\alpha 3}\boldsymbol{U}_h\right\} + \left\{\frac{\partial \boldsymbol{V}^\intercal}{\partial \xi_\alpha}\boldsymbol{Q}_{\alpha\beta} + \boldsymbol{V}^\intercal \boldsymbol{R}_{\beta 3}^\intercal\right\}[\![\boldsymbol{U}_h]\!]_\beta + \\ - \int_{\partial\Omega_{\xi D}^h} \nu_\alpha \boldsymbol{V}^\intercal\left(\boldsymbol{Q}_{\alpha\beta}\frac{\partial \boldsymbol{U}_h}{\partial \xi_\beta} + \boldsymbol{R}_{\alpha 3}\boldsymbol{U}_h\right) + \left(\frac{\partial \boldsymbol{V}^\intercal}{\partial \xi_\alpha}\boldsymbol{Q}_{\alpha\beta} + \boldsymbol{V}^\intercal \boldsymbol{R}_{\beta 3}^\intercal\right)\boldsymbol{U}_h \nu_\beta + \\ + \int_{\partial\Omega_{\xi I}^h} \mu [\![\boldsymbol{V}]\!]_\alpha^\intercal [\![\boldsymbol{U}_h]\!]_\alpha + \int_{\partial\Omega_{\xi D}^h} \mu \boldsymbol{V}^\intercal \boldsymbol{U}_h. \end{aligned} \tag{39}$$

4. Results

To validate the formulation presented in the preceding section, a few tests involving different geometries and several high-order ESL theories as well as DG basis functions are considered. The investigated geometries are a square plate, a cylindrical shell, and a NURBS-based shell. Two different materials are taken into account, namely an isotropic material and an orthotropic material, whose properties are reported in Tab.(1).

Table 2 – Properties of the considered shell sections.

Shell ID	Material	Layup	Layer(s) thickness
P_1	M_1	$[0]$	τ
P_2	M_2	$[0/90/0/90]$	$\tau/4$
C_1	M_1	$[0]$	τ
C_2	M_2	$[0/90/0/90]$	$\tau/4$
N_1	M_2	$[0/90/90/0]$	$\tau/4$

4.1 Square plate

The first investigated geometry is a square plate, whose mid-surface is defined as

$$\boldsymbol{x}_0 = \begin{bmatrix} \xi_1 \\ \xi_2 \\ 0 \end{bmatrix}, \tag{40}$$

where $\xi_1, \xi_2 \in [0, L]$, being L the length of the sides of the plate. Two plate sections are considered here, an isotropic plate P_1 and a laminated P_2 whose properties are reported in Tab.(2). The plate has a thickness ratio of $\frac{\tau}{L} = \frac{1}{100}$ and is subjected to simply-supported boundary conditions. The characteristic dimension of the mesh element h is then given by L_e/L, where L_e is the length of the side of each square elements.

Figure (2) shows the convergence of the error on the first natural frequency and on the first eigenfunction as for a given mesh size h and order p of the DG basis functions using the FSDT. The errors are defined as

$$e(\omega_h) \equiv \frac{\omega_h - \omega_{\mathrm{ref}}}{\omega_{\mathrm{ref}}}, \tag{41a}$$

$$e(\boldsymbol{U}_h) \equiv \frac{|\boldsymbol{U}_h - \boldsymbol{U}_{\mathrm{ref}}|_\infty}{|\boldsymbol{U}_{\mathrm{ref}}|_\infty}, \tag{41b}$$

where the subscript ref denotes exact solution quantities and the subscript h denotes the quantities computed with the proposed DG formulation.

Four different ESL theories are then taken into account and the corresponding first ten non-dimensional frequencies are computed for the plate P_2 using an order $p = 6$ of the DG basis functions and a 4×4 structured grid. The non-dimensional frequencies are computed as

$$\overline{\omega} \equiv \frac{L^2}{\pi^2}\sqrt{\frac{\rho_r}{E_r \tau^2}}\omega, \tag{42}$$

The obtained values are reported in Tab.(3) and compared with the analytical solutions, showing excellent matching.

As the last test, the transient response of the plate P_2 is investigated. The plate starts from an undeformed configuration and is subjected to simply-supported boundary conditions and to a pressure on the lower surface whose expression is $q_0 \sin(\pi\xi_1/L)\sin(\pi\xi_2/L)H(t)$, where $H(t)$ is the Heaviside step function.

The transient response of the plate is reported in terms on the third non-dimensional component $\overline{u}_{\xi_3}$ of the displacement vector defined as

$$\overline{u}_{\xi_3} \equiv \frac{\tau^3 E_r}{L^4 q_0} u_{\xi_3}. \tag{43}$$

Figure (3) shows the computed value of $\overline{u}_{\xi_3}$ at the point of coordinates $(L/2, L/2, 0)$ as a function of time t and order p of the DG basis functions using a 2×2 structured grid; in the figure, T_n is the period of free-vibration of the half-wave bending mode while the dashed line denotes the exact solution, which is accurately recovered for $p > 2$.

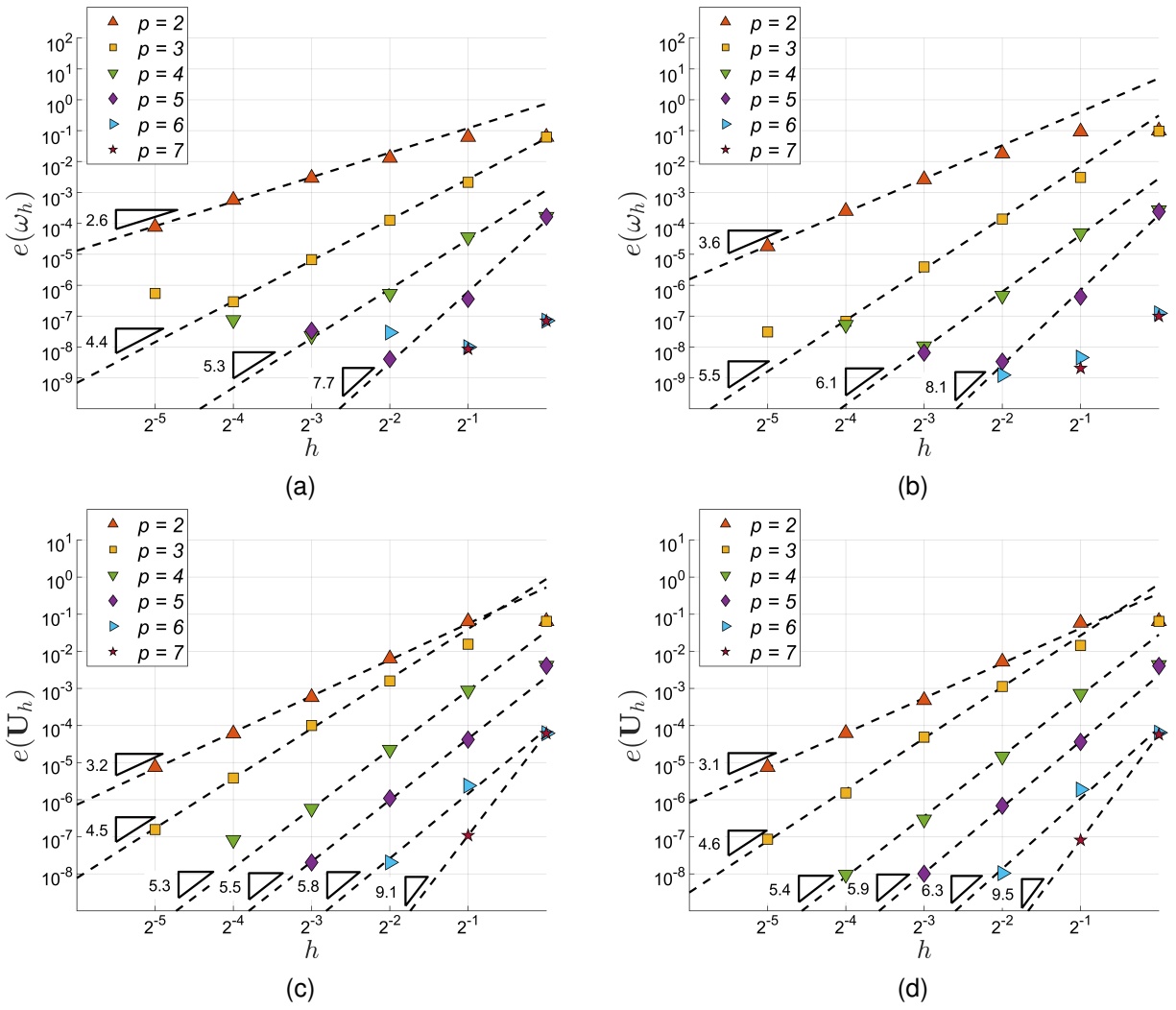

Figure 2 – hp-convergence of the error on the first natural frequency for the plate P_1 (a) and P_2 (b), and on the first eigenfunction for the plate P_1 (c) and P_2 (d)

Table 3 – First ten natural frequencies for the plate P_2.

	FSDT (DG)	FSDT $(S.A.)$	ED_{111} (DG)	ED_{111} $(S.A.)$	ED_{222} (DG)	ED_{222} $(S.A.)$	ED_{333} (DG)	ED_{333} $(S.A.)$
$\overline{\omega}_1$	1.4211	1.4211	1.4311	1.4311	1.4214	1.4214	1.4207	1.4207
$\overline{\omega}_2$	4.0147	4.0147	4.0398	4.0398	4.0181	4.0181	4.0108	4.0108
$\overline{\omega}_3$	4.0147	4.0147	4.0398	4.0398	4.0181	4.0181	4.0108	4.0108
$\overline{\omega}_4$	5.6537	5.6537	5.6981	5.6981	5.6593	5.6593	5.6483	5.6483
$\overline{\omega}_5$	8.6321	8.6321	8.6899	8.6899	8.6481	8.6481	8.6125	8.6125
$\overline{\omega}_6$	8.6321	8.6321	8.6899	8.6899	8.6481	8.6481	8.6125	8.6125
$\overline{\omega}_7$	9.6535	9.6535	9.7320	9.7320	9.6710	9.6710	9.6343	9.6343
$\overline{\omega}_8$	9.6535	9.6535	9.7320	9.7320	9.6710	9.6710	9.6343	9.6343
$\overline{\omega}_9$	12.6091	12.6091	12.7243	12.7243	12.6363	12.6363	12.5823	12.5823
$\overline{\omega}_{10}$	15.0412	15.0412	15.1619	15.1619	15.0891	15.0891	14.9808	14.9808

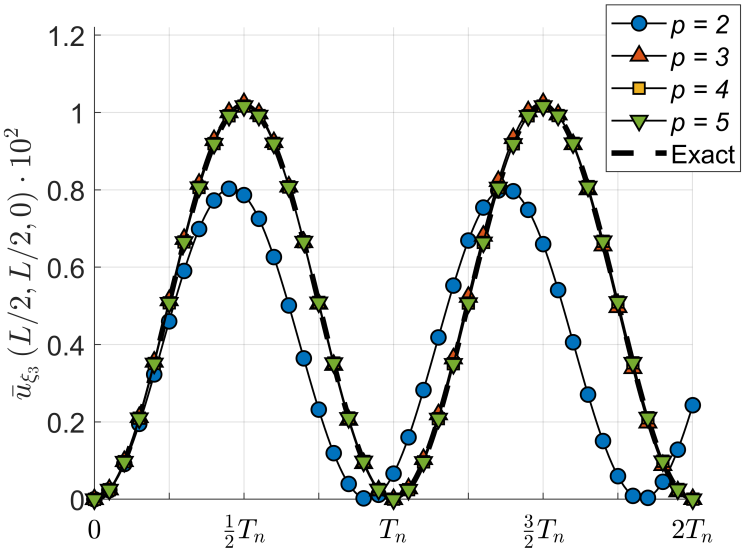

Figure 3 – Dynamic response of the plate P_2.

4.2 Cylindrical shell

The second investigated geometry is that of cylindrical shell. The map of the mid-surface is given as

$$\boldsymbol{x}_0 = \begin{bmatrix} R\cos(\xi_1) \\ R\sin(\xi_1) \\ \xi_2 \end{bmatrix}, \tag{44}$$

where R denotes the radius of the cylindrical shell. The first curvilinear coordinate for this geometry takes values in $[0, \alpha]$, being $\alpha = 1$ rad, and the second one takes values in $[0, L]$. The considered shell sections are those denoted by C_1 and C_2 in Tab.(2) and consist of an isotropic single-layer and a laminated cross-ply section, respectively. The thickness ratio is $\frac{\tau}{L} = \frac{1}{100}$ and the shell is subjected to simply supported boundary conditions. Fig.(4) shows the convergence of the error on the first natural frequency and on the first eigenfunction computed using Eq.(41) as functions of the order p of the DG basis functions and the mesh size h. The shell theory used in these tests is the FSDT.
In the second set of tests, the values of the first ten non-dimensional natural frequencies for the shell C_2 are computed using an order $p = 6$ of the DG basis functions and a 4×4 structured grid. The values are compared with those obtained analytically in Tab.(4) showing excellent matching also in this case. The non-dimensional values of the frequencies are computed as in Eq.(42). For the last test, starting from an undeformed configuration, the shell C_2 is subjected to an internal pressure varying as $q_0 \sin(\pi\xi_1/\alpha)\sin(\pi\xi_2/L)H(t)$. The value of the non-dimensional third covariant component of the displacement vector $\overline{u}_{\xi_3}$ is computed as a function of time using different order of the DG basis functions and a 2×2 grid. Figure (5) shows the obtained results, which match very well with the analytical solution for $p > 2$.

4.3 NURBS-based shell

The last investigated geometry is a generally-curved NURBS-based shell with a cut-out as shown in Fig.(6). The detailed description of the geometry can be found in [24], where the information for the definition of the NURBS-surface, such as the coordinates of the control points or the elements of the knot vector, is provided. Nevertheless, the main geometrical measures are recalled here in Tab.(5) for the sake of completeness. The level set function used for the cut-out is defined in Cartesian coordinates as

$$\phi(\boldsymbol{x}_0) = a^d - |x_{01} - x_{1n}|^d - |x_{02} - x_{2n}|^d, \tag{45}$$

where the values of a, d, x_{1n}, and x_{2n} are reported in Tab.(5) and x_{01} and x_{02} are the Cartesian coordinates of a generic point on the mid-surface. Using the map of the reference surface of the shell the level set is transformed into a function of the curvilinear variables and it is used to generate

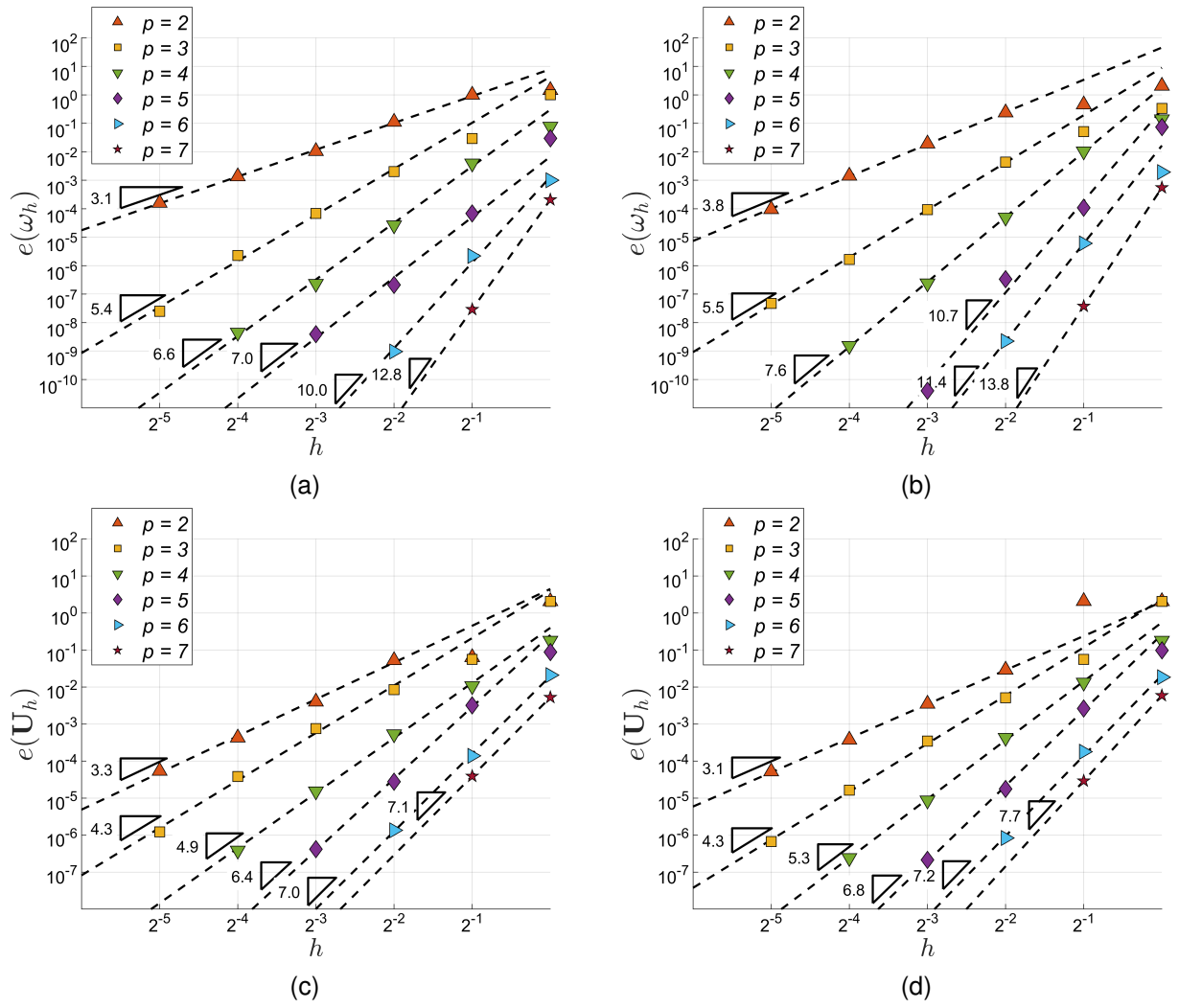

Figure 4 – hp-convergence of the error on the first natural frequency for the shell C_1 (a) and C_2 (b), and on the first eigenfunction for the shell C_1 (c) and C_2 (d).

Table 4 – First ten natural frequencies for the shell C_2.

	FSDT (DG)	FSDT $(S.A.)$	ED_{111} (DG)	ED_{111} $(S.A.)$	ED_{222} (DG)	ED_{222} $(S.A.)$	ED_{333} (DG)	ED_{333} $(S.A.)$
$\overline{\omega}_1$	5.1031	5.1031	5.1210	5.1210	5.0987	5.0987	5.0933	5.0933
$\overline{\omega}_2$	6.7424	6.7424	6.7442	6.7442	6.7418	6.7418	6.7417	6.7417
$\overline{\omega}_3$	8.7785	8.7785	8.8269	8.8269	8.7801	8.7801	8.7456	8.7456
$\overline{\omega}_4$	8.7999	8.7999	8.8317	8.8317	8.7999	8.7999	8.7931	8.7931
$\overline{\omega}_5$	10.5801	10.5801	10.6484	10.6484	10.5852	10.5852	10.5522	10.5522
$\overline{\omega}_6$	13.3841	13.3841	13.3911	13.3911	13.3852	13.3852	13.3832	13.3832
$\overline{\omega}_7$	13.8991	13.8991	13.9523	13.9523	13.9102	13.9102	13.8851	13.8851
$\overline{\omega}_8$	14.2770	14.2770	14.3763	14.3763	14.2946	14.2946	14.2474	14.2474
$\overline{\omega}_9$	15.0348	15.0348	15.1503	15.1503	15.0621	15.0621	14.9537	14.9537
$\overline{\omega}_{10}$	16.0497	16.0497	16.1837	16.1837	16.0801	16.0801	15.9738	15.9738

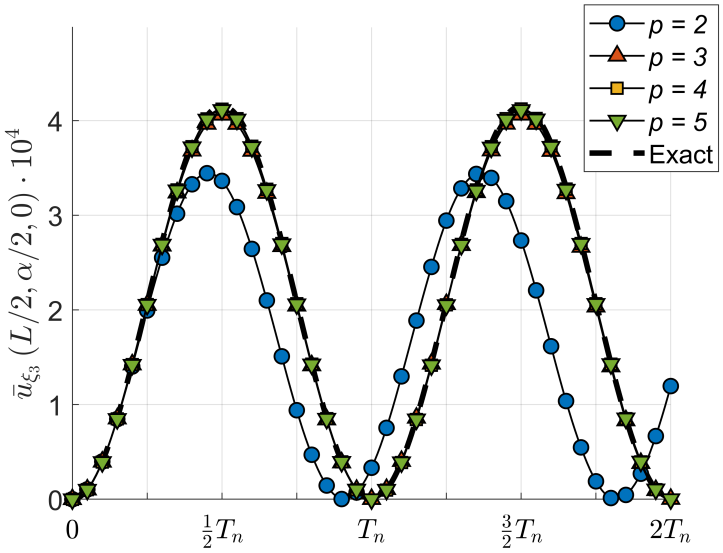

Figure 5 – Dynamic response of the shell C_2.

Table 5 – Geometrical parameters for the NURBS-based generally-curved shell.

NURBS-based shell	
H	50 cm
D	5 cm
L	60 cm
a	8.5 cm
d	3
x_{1n}	15 cm
x_{2n}	12 cm
τ	1 mm

the implicit mesh. The shell is subjected to clamped boundary conditions on the external boundary while the boundary of the cut-out is traction-free. In the first set of tests, the first six free-vibration modes in terms of the magnitude of the displacement are evaluated using a 10×10 background grid and a $p = 6$ for the order of the DG basis functions. The obtained results are compared with those computed using Abaqus' S3 elements; the comparison is reported in Fig.(7) showing the accuracy of the present approach.

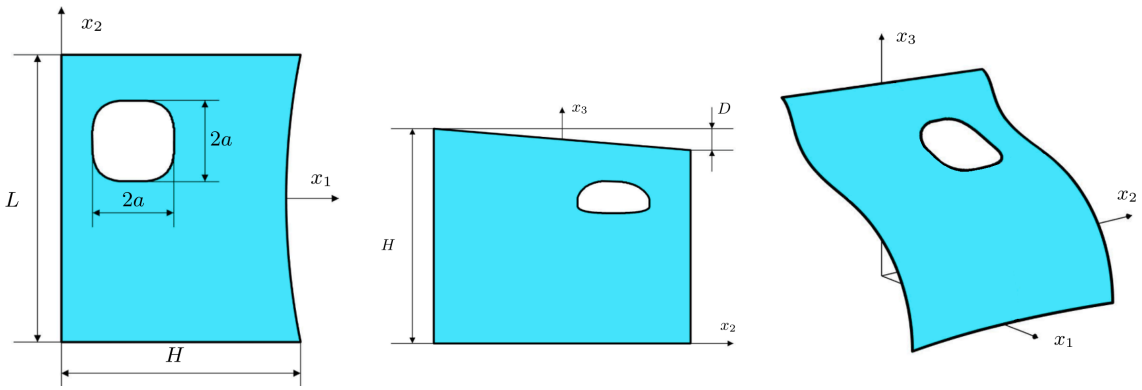

(a) (b) (c)

Figure 6 – Geometry of the NURBS-based shell in three different views.

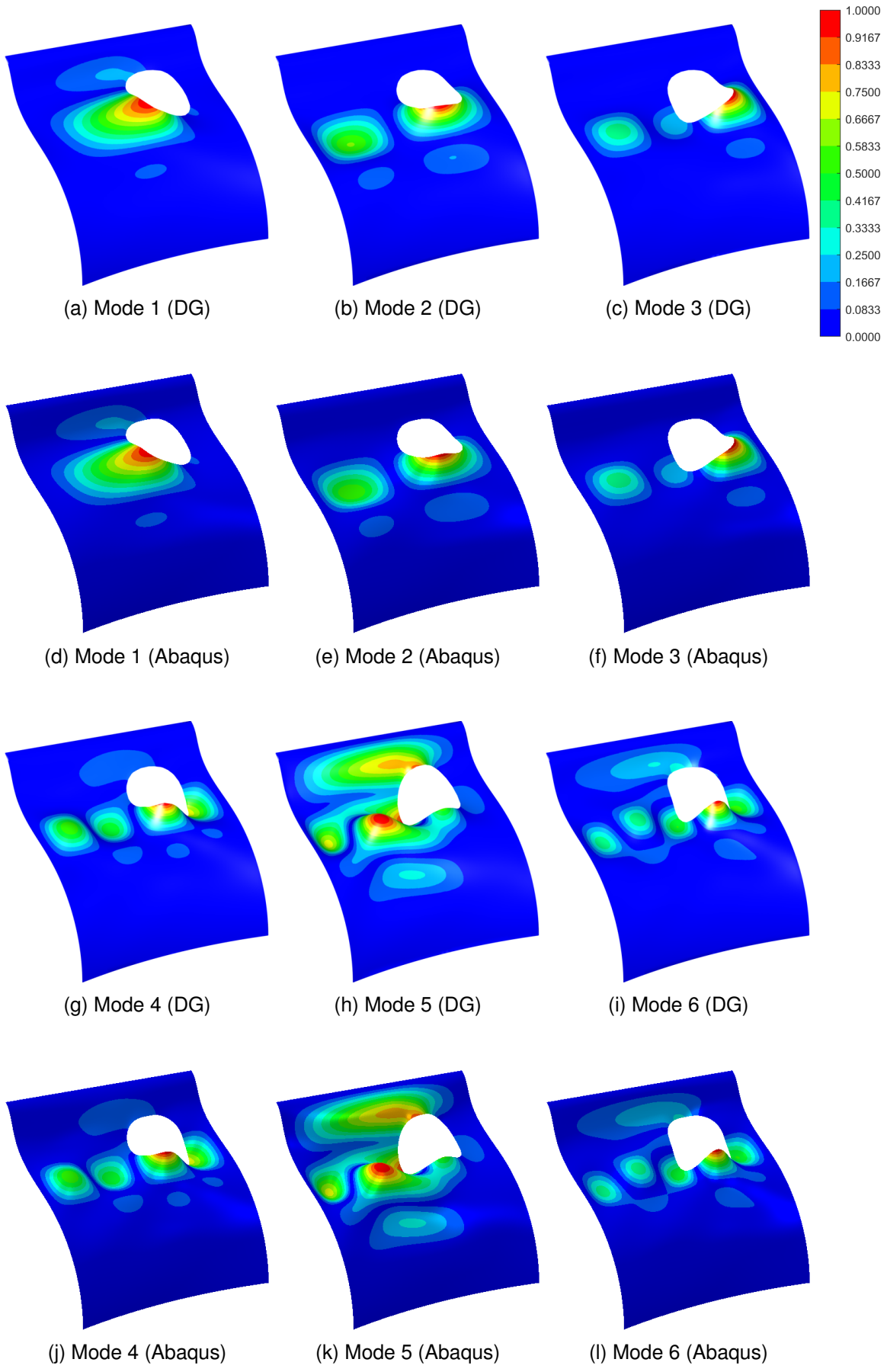

(a) Mode 1 (DG) (b) Mode 2 (DG) (c) Mode 3 (DG)

(d) Mode 1 (Abaqus) (e) Mode 2 (Abaqus) (f) Mode 3 (Abaqus)

(g) Mode 4 (DG) (h) Mode 5 (DG) (i) Mode 6 (DG)

(j) Mode 4 (Abaqus) (k) Mode 5 (Abaqus) (l) Mode 6 (Abaqus)

Figure 7 – First six free-vibration modes for the shell N_1 computed using DG (a-c and g-i) and Abaqus S3 elements (d-f and j-l).

The last set of tests concerns the transient response of the NURBS-based shell when subjected to a uniform pressure $q_0 H(t)$ applied onto the internal surface. In this case, a damped analysis is considered and the damping ratios for the first and sixth free-vibration mode are selected as $\zeta_1 = \zeta_6 = 0.1$. Figure (8) shows the non-dimensional magnitude of the displacement for the point with curvilinear coordinates $\xi_1 = \alpha = 0.3922$ and $\xi_2 = \beta = 0.5808$ as a function of time $0 < t < 5T_n$, where T_n is the period of the first free-vibration frequency.

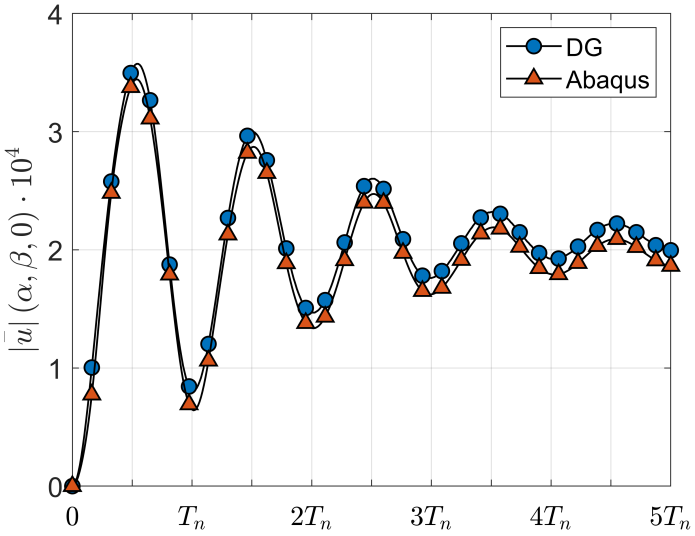

Figure 8 – Dynamic response of the shell N_1.

5. Conclusion

In this work, an Interior Penalty discontinuous Galerkin formulation for the free-vibration and transient analysis of laminated composite shells has been proposed. The ESL approach is used for the covariant components of the displacement vector along the shell thickness. The mid-surface of the shell is described using either analytical or NURBS-based surfaces. The presence of a cut-out is resolved through the implicit-mesh approach, whereby a level-set function, that implicitly defines the reference domain, is combined with a background rectangular grid to generate the mesh. The efficiency of the formulation has been assessed through multiple tests on different geometries. The first two sets of tests where conducted on a square plate and on a cylindrical shell. These tests admit analytical solutions and have allowed us to demonstrate the high-order accuracy of the formulation. The last set of tests were conducted on a NURBS-based shell. The contour plot of the displacement magnitude for the first six free-vibration modes and the transient response of the structure were compared with Abaqus results, showing the capability of the proposed approach to accurately reproduce the free-vibration and transient response of generally curved shells. In general, in all the conducted tests, the results obtained with method proposed show excellent agreement with the reference ones, demonstrating the potential of the formulation for being used as an efficient tool for transient and free-vibration analysis of shell structures.

6. Contact Author Email Address

mailto: alberto.milazzo@unipa.it

7. Copyright Statement

References

[1] Carrera E and Zappino E. Carrera Unified Formulation for Free-Vibration Analysis of Aircraft Structures. *AIAA Journal*, Vol. 54, No. 1, pp 280-292, 2016.

[2] Guo J, Shi D, Wang Q, Tang J and Shuai C. Dynamic analysis of laminated doubly-curved shells with general boundary conditions by means of a domain decomposition method. *International Journal of Mechanical Sciences*, Vol. 138–139, pp 159-186, 2018.

[3] Wang Q, Shao D and Qin B. A simple first-order shear deformation shell theory for vibration analysis of composite laminated open cylindrical shells with general boundary conditions. *Composite Structures*, Vol. 184, pp 211-232, 2018

[4] Sciascia G, Oliveri V, Milazzo A and Weaver P M. Ritz solution for transient analysis of variable-stiffness shell structures. *AIAA Journal*, Vol. 58, No. 4, pp 1796-1810, 2020.

[5] Van Do V N and Lee CH. Free vibration and transient analysis of advanced composite plates using a new higher-order shear and normal deformation theory. *Archive of Applied Mechanics*, Vol. 91, pp 1793–1818, 2021.

[6] Carrera, E. Theories and finite elements for multilayered, anisotropic, composite plates and shells. *Archives of Computational Methods in Engineering*, Vol. 9, No. 2, pp 87-140, 2002.

[7] Reddy JN and Phan ND. Stability and vibration of isotropic, orthotropic and laminated plates according to a higher-order shear deformation theory. *Journal of sound and vibration*, Vol. 98, No. 2, pp 157-170, 1985.

[8] Arnold D N, Brezzi F, Cockburn B and Marini L D. Unified analysis of discontinuous Galerkin methods for elliptic problems. *SIAM journal on numerical analysis*, Vol. 39, No. 5, pp 1749-177, 2002.

[9] Antonietti P F and Mazzieri I. High-order discontinuous Galerkin methods for the elastodynamics equation on polygonal and polyhedral meshes. *Computer Methods in Applied Mechanics and Engineering*, Vol. 342, pp 414-437, 2018.

[10] Gulizzi V, Benedetti I and Milazzo A. An implicit mesh discontinuous galerkin formulation for higher-order plate theories. *Mechanics of Advanced Materials and Structures*, Vol. 27, No. 17, pp 1494–1508, 2020.

[11] Gulizzi V and Saye R. Modeling wave propagation in elastic solids via high-order accurate implicit-mesh discontinuous Galerkin methods. *Computer Methods in Applied Mechanics and Engineering*, Vol. 395, pp 114971, 2022.

[12] Noels L and Radovitzky R. A new discontinuous Galerkin method for Kirchhoff–Love shells. *Computer Methods in Applied Mechanics and Engineering*, Vol. 197, No. 33-40, pp 2901-2929, 2008.

[13] Noels L. A discontinuous Galerkin formulation of non-linear Kirchhoff–Love shells *International Journal for Numerical Methods in Engineering*, Vol. 78, pp 296-323, 2009.

[14] Talamini B L and Radovitzky R. A discontinuous Galerkin method for nonlinear shear-flexible shells. *Computer Methods in Applied Mechanics and Engineering*, Vol. 303, pp 128-162, 2016.

[15] Benedetti I, Gulizzi V, and Milazzo A. Layer-Wise Discontinuous Galerkin Methods for Piezoelectric Laminates. *Modelling*, Vol. 1, No. 2, pp 198-214, 2020.

[16] Antonietti P F, Buffa A, Perugia I. Discontinuous Galerkin approximation of the Laplace eigenproblem. *Computer methods in applied mechanics and engineering*. Vol. 195. No. 25-28, pp. 3483-3503, 2006.

[17] Buffa A, and Perugia I. Discontinuous Galerkin approximation of the Maxwell eigenproblem. *SIAM Journal on Numerical Analysis* Vol. 44, No. 5, pp 2198-2226, 2006.

[18] Buffa A, Houston P, Perugia I. Discontinuous Galerkin computation of the Maxwell eigenvalues on simplicial meshes. *Journal of Computational and Applied Mathematics*. Vol. 204. No. 2, pp. 317-333, 2007.

[19] Guarino G, Milazzo A, and Gulizzi V. Buckling analysis of multilayered structures using high-order theories and the implicit-mesh discontinuous Galerkin method. *AIAA SCITECH 2022 Forum*, San Diego, 1490, 2022.

[20] Saye R. Implicit mesh discontinuous Galerkin methods and interfacial gauge methods for high-order accurate interface dynamics, with applications to surface tension dynamics, rigid body fluid–structure interaction, and free surface flow: Part I. *Journal of Computational Physics*, Vol. 344, pp 647-682, 2017

[21] Saye R. High-order quadrature methods for implicitly defined surfaces and volumes in hyperrectangles. *SIAM Journal on Scientific Computing*, Vol. 37, No. 2, pp A993-A1019

[22] Ciarlet P G. An introduction to differential geometry with applications to elasticity. *Journal of Elasticity*, Vol. 78, No. 1-3, pp 1–215, 2005.

[23] Liu M and Gorman D G. Formulation of Rayleigh damping and its extensions. *Computers & structures*, Vol. 57, No. 2, pp 277-285, 1995

[24] Guarino G, Gulizzi V and Milazzo A. High-fidelity analysis of multilayered shells with cut-outs via the discontinuous Galerkin method. *Composite Structures*, Vol. 276, 114499, 2021.

[25] Gulizzi V, Benedetti I and Milazzo A. A high-resolution layer-wise discontinuous Galerkin formulation for multilayered composite plates. *Composite Structures*, Vol. 242, pp 112137, 2020.

[26] Guarino G, Milazzo A and Gulizzi V. Equivalent-single-layer discontinuous galerkin methods for static analysis of multilayered shells. *Applied Mathematical Modelling*, Vol. 98, pp 701-721, 2021.

[27] Reddy JN. *Mechanics of laminated composite plates and shells: theory and analysis*. CRC press. 2003.

[28] Rogers DF. *An introduction to NURBS: with historical perspective*. Morgan Kaufmann, 2001.

[29] Piegl L and Tiller W. *The NURBS book*. Springer Science & Business Media, 1996.

[30] Ting T. *Anisotropic elasticity: theory and applications*. Oxford Engineering Science Series. 1996

[31] Jones R M. *Mechanics of composite materials*. CRC Press, 2018.

[32] Bathe K J. *Finite element procedures*. Prentice-Hall, 1996.